

A Central Motor System Inspired Pre-training Reinforcement Learning for Robotic Control

Pei Zhang, Zhaobo Hua, Jinliang Ding, *Senior Member, IEEE*

Abstract—Designing controllers to achieve natural motor capabilities for multi-joint robots is a significant challenge. However, animals in nature are naturally with basic motor abilities and can master various complex motor skills through acquired learning. On the basis of analyzing the mechanism of the central motor system in mammals, we propose a novel pre-training reinforcement learning algorithm that enables robots to learn rich motor skills and apply them to complex task environments without relying on external data. We first design a skill based network similar to the cerebellum by utilizing the selection mechanism of voluntary movements in the basal ganglia and the basic motor regulation ability of the cerebellum. Subsequently, by imitating the structure of advanced centers in the central motor system, we propose a high-level policy to generate different skill combinations, thereby enabling the robot to acquire natural motor abilities. We conduct experiments on 4 types of robots and 22 task environments, and the results show that the proposed method can enable different types of robots to achieve flexible motor skills. Overall, our research provides a promising framework for the design of neural network motor controllers.

Index Terms—Basal ganglia, central motor system, motor control, neuroscience, reinforcement learning (RL).

I. INTRODUCTION

ENABLING robots to have universal, flexible, and adaptive motor capabilities in complex environments has always been a significant challenge, and reinforcement learning (RL) emerges as an important and feasible way to address this challenge [1] [2]. Through carefully designed reward functions, robots can acquire flexible motor abilities [3] [4]. However, traditional reinforcement learning methods usually focus on learning specific tasks, resulting in limited generalization ability of motor controllers and insufficient flexibility in the generated actions. Once the task changes, the controller needs to be retrained.

In fields such as computational vision, researchers advocate the use of large-scale data to obtain universal models, thereby enabling intelligent agents to quickly adapt to downstream tasks [5]. Combining this pre-training method with hierarchical reinforcement learning [6], pre-training RL has made progress

in designing smart robot motor controllers. Unsupervised reinforcement learning methods encourage robots to collect different experiences and evolve diverse skills through intrinsic rewards [7], enabling them to quickly adapt to downstream tasks. Under unsupervised conditions, the exploration ability of agents is greatly improved, but they will develop skills unrelated to downstream tasks. Goal space conditioned approaches balance exploration efficiency and universality by establishing a specialized goal space during pre-training, but the design of the goal space requires a large amount of expert knowledge [8]. On the contrary, data-driven methods enable robots to generate highly lifelike actions by learning from a large amount of collected data. For example, adversarial skill embedding is a promising method that uses unstructured motion clips to train a low-level latent variable model [9], allowing robots to generate actions similar to the dataset. But obtaining and maintaining such datasets can be a costly task.

Although these methods have made significant progress in motor control, they still cannot achieve animal like motor abilities. In nature, mammals are born with some basic natural motor abilities (such as balance, crawling, etc.). Through learning, they will acquire more complex skills to solve tasks in various scenarios. The natural motor ability of animals mainly comes from their central motor system (CMS) [10], which has a natural three-level structure [11]. The highest level is responsible for generating complex motor strategies. The middle layer participates in the formation of ordered control signals, while the lowest layer is responsible for executing actions. The system has partial autonomy, even if some higher level organs are removed, lower level systems can still operate [12] [13]. But more complex behaviors require high level systems to repeatedly call lower level systems to implement (repeatability). This hierarchical relationship also reflects both state abstraction and temporal abstraction [14] [15].

Inspired by these properties, this article designs a pre-training reinforcement learning algorithm based on central motor system (CMSRL) to solve the problems of current methods and enable robots to acquire more natural motor abilities. Specifically, we first train a low-level skill latent space model similar to the cerebellum. It can generate diverse motor behavior patterns with different levels of activity based on different skills. More importantly, even if effective skill information is not received, the low-level policy can still enable the robot to maintain basic movement abilities. In order to generate behavior patterns at different levels of activity, we first design a new skill encoding method, and then design the corresponding decoding method and skill activity calculation function based on the regulatory mechanism of

This work was supported in part by the National Natural Science Foundation of China under Grant 61988101, the National Key R&D Plan Project under Grant 2022YFB3304700, the 111 Project 2.0 under Grant B08015, and the Liaoning Province Central Leading Local Science and Technology Development Special Project under Grant 2022JH6/100100055. (Corresponding author: Jinliang Ding)

P. Zhang and Z. Hua, and J. Ding are with the State Key Laboratory of Synthetical Automation for Process Industries, Northeastern University, Shenyang 110819, China (email: pei.zhang088@outlook.com; Bobby_1752635630@outlook.com; jlding@mail.neu.edu.cn).

Parts of the figure were drawn by using pictures from Servier Medical Art. Servier Medical Art by Servier is licensed under a Creative Commons Attribution 3.0 Unported License (<https://creativecommons.org/licenses/by/3.0/>).

the basal ganglia. The encoder encodes discrete skills into a low dimensional latent space, while the decoder is responsible for recovering skill information. The skill activity calculation function then assign activity values to the decoded skills and use them as weights for RL rewards. On the other hand, diverse motor patterns are achieved by maximizing the mutual information. The autonomy of the low-level policy comes from the basic motor reward we designed. After training, the latent skill space can serve as an abstract action space for the high-level policy to participate in the next stage of the training process. With the coordination of two-level policies, the model can generate naturally agile behavior without relying on any external data.

We demonstrate the effectiveness of the proposed approach on four different robots and six different tasks. Compared with baselines, CMSRL has better performance in complex task environments. The natural movement ability of robots also proves the effectiveness of CMS mechanisms in reinforcement learning. To summarize, This study makes the following contributions.

- 1) A new pre-training reinforcement learning framework CMSRL based on the CMS architecture that enables robots to acquire the ability to solve complex tasks.
- 2) A new skill encoding method that can maximize the differences between different skills.
- 3) A skill decoding method and an skill activity calculation function based on the motor regulation function of the basal ganglia.
- 4) A new reinforcement learning reward function that enables robots to simultaneously possess basic motor abilities and multiple adjustable motor patterns.

The rest of this article is organized as follows. Section II and Section III present relevant research progresses and preliminaries. Section IV presents our main contributions. The results of the simulation experiments are presented in Section V. Finally, the conclusion is summarized in Section VI.

II. RELATED WORK

Recent work in the field of pre-training RL can be divided into three groups based on the methods used: unsupervised reinforcement learning, goal space conditioned learning, and data-driven learning.

A. Unsupervised Reinforcement Learning

Unsupervised reinforcement learning enables agents to collect different experiences and self learn useful skills in the environment through intrinsic rewards. According to the composition of intrinsic rewards, these studies can be divided into three types: data-based, skill-based, and knowledge-based.

1) Data-based methods mainly explore data diversity by maximizing data coverage. Liu & Abbeel [16] presented the Active Pre-Training algorithm (APT), which conducts environmental exploration by maximizing a non-parametric entropy calculated within an abstract representation space. By designing a new PD loss with prescription gap maximization (PGM) loss and Jacobian regularization (JR) loss, Qu et al. [17] proposed a robust DRL paradigm unknown to the

opponent and verified the method's superiority in experiments. Pina et al. [18] proposed a new Residual Q-Network (RQN) concept to address the increasing environmental complexity in MARL research. This method transforms individual Q-value trajectories by preserving the individual-global-max criteria. These approaches are designed to generalize various tasks while accelerating subsequent exploration for more efficient task-specific training, which can achieve better performance and robustness in the complex environment particularly.

2) The skill-based approach primarily achieves skill diversity by maximizing mutual information between states s and skills z . Park et al. [19] introduced LSD, a method that incentivizes the agent to explore a broader spectrum of diverse and dynamic skills with extended reach. Eysenbach et al. [20] introduced DIAYN, which optimizes information theory objectives through maximum entropy policy to achieve skill learning, providing a solution for solving exploration challenges and improving data efficiency in reinforcement learning. Liu & Abbeel [21] introduced APS by reinterpreting and merging variational successor features [22] with non-parametric entropy maximization [16]. APS overcomes the constraints of current unsupervised RL methods based on mutual information maximization and entropy maximization, effectively amalgamating the strengths of both approaches.

3) The knowledge-based method increases the agent's understanding of the world by maximizing prediction errors. Pathak et al. [23] presented ICM, a method that leverages curiosity as an intrinsic reward signal, enabling the agent to investigate its surroundings and acquire valuable skills. Sekar et al. [24] proposed Plan2Explore, which allows agents to quickly adapt to multiple downstream tasks in zero or few-shot after exploration.

B. Goal Space Conditioned Learning

Although unsupervised learning can accelerate the adaptation speed of intelligent agents to downstream tasks, it is difficult to balance skill universality and sampling efficiency. The Goal space method is a compromise approach; by designing appropriate skill spaces, a balance can be achieved between them. Gehring et al. [8] alleviated the need for prior knowledge by proposing a hierarchical skill learning framework that acquires skills of varying complexity in an unsupervised manner. Shi et al. [25] proposed a novel reinforcement learning based approach that consists of a foot trajectory generator. This generator continuously optimizes given tasks to provide different motion priors to guide policy learning. To handle tasks with dynamic obstacles, Bing et al. [26] used environmental image observations to select hindsight goals and proposed a bounding-box-based hindsight goal generation (Bbox HGG). The disadvantage of these methods is that the goal space is difficult to design, requiring extensive expert knowledge and repeated experiments.

C. Data-Driven Learning

The above two methods have shown good results in low dimensional space. However, for complex robots with higher degrees of freedom, relying solely on unsupervised or goal

space design makes it difficult to achieve natural motor effects. Learning motor skills from data effectively solves the motor control of the high degree of freedom multi-joint robots. Modares et al. [27] presented a data-driven safe reinforcement learning algorithm for discrete-time nonlinear systems, which directly learns a robust security proof while completely bypassing the recognition of the system model and ensuring the safety and stability of agent behavior. Park et al. [28] presented a network-based algorithm that learns control policies from unorganized, minimally-labeled human motion data. Peng et al. [29] adopted a two-level hierarchical control framework to learn various environment-aware locomotion skills with a limited amount of prior knowledge. Although the above methods can learn the target policy from limited prior knowledge, they still need to learn from scratch. Combining techniques from adversarial imitation learning and unsupervised reinforcement learning, Peng et al. [9] presented a large-scale data-driven framework ASE for learning versatile and reusable skill embeddings for physically simulated characters. This method does not require learning from scratch and can embed various skills. However, such methods' difficulty lies in the high cost of obtaining and maintaining motion capture data.

III. PRELIMINARY

A. Reinforcement Learning

Reinforcement learning is an optimization method based on Markov Decision Processes (MDP) $\langle \mathcal{S}, \mathcal{A}, p, r \rangle$, where \mathcal{S} represents the state space, \mathcal{A} represents the action space, p is the probability of transition from one state to another after executing an action, and r represents the reward function. At each time step t , the environment provides a state \mathbf{s}_t to a policy π , then the policy generates an action $\mathbf{a}_t \sim \pi(\mathbf{a}_t | \mathbf{s}_t)$ based on the state [1]. The environment executes \mathbf{a}_t and generates the next state $\mathbf{s}_{t+1} \sim p(\mathbf{s}_{t+1} | \mathbf{s}_t, \mathbf{a}_t)$ and a reward $r_t = r(\mathbf{s}_t, \mathbf{a}_t, \mathbf{s}_{t+1})$. From the state \mathbf{s}_t at time t until the termination state, the sum of all discounted rewards is called the return G_t , and the function of the return is given by the following equation, where γ is the discount factor between 0 and 1.

$$G_t = \sum_{k=0}^{\infty} \gamma^k r_{t+k}. \quad (1)$$

The value $V_\pi(\mathbf{s}_t)$ of state \mathbf{s}_t is defined as the mathematic expectation $\mathbb{E}_\pi[G_t | \mathbf{S}_t = \mathbf{s}_t]$ of the return G_t from that state to the termination state. Reinforcement learning seeks the optimal policy by maximizing the return expectation starting from the initial state \mathbf{s}_0 . The time horizon of the reinforcement learning process in this article is finite. Within a certain time step T , the policy will generate a finite trajectory $\tau = \langle \mathbf{s}_0, \mathbf{a}_0, \mathbf{s}_1, r_0, \dots, \mathbf{s}_{T-1}, \mathbf{a}_{T-1}, \mathbf{s}_T, r_{T-1} \rangle$, the goal of RL is to find the optimal policy π^* to maximize the following objective function

$$J(\pi) = \mathbb{E}_{\tau \sim \pi} \left[\sum_{t=0}^{T-1} \gamma^t r_t \right]. \quad (2)$$

B. Unsupervised Pre-Training RL

In unsupervised pre-training RL, the agent trains in MDP $\langle \mathcal{S}, \mathcal{A}, p, \mathcal{Z} \rangle$ without external rewards, where \mathcal{Z} represents the skill space. Given a skill \mathbf{z} and a policy $\pi(\mathbf{a}_t | \mathbf{s}_t, \mathbf{z})$, the trajectory $\tau = \langle \mathbf{s}_0, \mathbf{a}_0, \mathbf{s}_1, \dots, \mathbf{s}_{T-1}, \mathbf{a}_{T-1}, \mathbf{s}_T \rangle$ can be obtained during the T -step interaction between the agent and the environment. The goal of this method is to enable agents to quickly adapt to downstream environments by maximizing intrinsic rewards r_z during the process.

Using mutual information (MI) as r_z is a promising approach [16] [20]. The core idea of this method is to maximize the mutual information between the state \mathbf{s} generated by policy π and skill \mathbf{z} , thereby encouraging agents to correspond different skills to different states. MI rewards can be expressed as follows

$$\begin{aligned} I(\mathbf{s}; \mathbf{z} | \pi) &= I(\mathbf{z}; \mathbf{s} | \pi) \\ &= -\mathbb{E}_{p(\mathbf{z})} [\log p(\mathbf{z})] + \mathbb{E}_{p(\mathbf{z})} \mathbb{E}_{p(\mathbf{s} | \pi, \mathbf{z})} [\log p(\mathbf{z} | \mathbf{s}, \pi)]. \end{aligned} \quad (3)$$

Calculating $p(\mathbf{z} | \mathbf{s}, \pi)$ during training is a tricky task. We can introduce $q(\mathbf{z} | \mathbf{s})$ as a variational approximation for this value, where q can be updated by the posterior data \mathbf{z} generated during the training process [30]. From $\mathcal{H}(p) \leq \mathcal{H}(p, q)$, the following equation can be obtained

$$\begin{aligned} I(\mathbf{s}; \mathbf{z} | \pi) &\geq -\mathbb{E}_{p(\mathbf{z})} [\log p(\mathbf{z})] + \mathbb{E}_{p(\mathbf{z})} \mathbb{E}_{p(\mathbf{s} | \pi, \mathbf{z})} [\log q(\mathbf{z} | \mathbf{s})]. \end{aligned} \quad (4)$$

Therefore, the intrinsic reward r_z can be recorded as

$$r_{z_t} = \log p(\mathbf{z}) + \log q(\mathbf{z} | \mathbf{s}_{t+1}), \quad (5)$$

then use the collected trajectory to find the optimal policy π^* by maximizing the following objective:

$$J(\pi) = \mathbb{E}_{\tau \sim \pi} \left[\sum_{t=0}^{T-1} \gamma^t r_{z_t} \right]. \quad (6)$$

IV. PROPOSED APPROACH

Our research focuses on seamlessly integrating the CMS with unsupervised pre-training RL to design an intelligent hierarchical reinforcement learning algorithm. In this section, we first analyze the operating mechanism of the CMS. We then propose the CMSRL algorithm framework and provide theoretical explanations for each module.

A. Central Motor System Abstract Structure

The hierarchical mechanism of the CMS can be described in Fig.1, with different control hierarchy levels distinguished by varying colors. The blue boxes represent the highest level, the yellow boxes represent the middle level, and the brown boxes represent the lowest level. In addition, the gray dashed boxes in the figure are used to represent the perceptual input areas related to motor control, while the elliptical shapes represent some brain structures related to information transmission. The process of making decisions by the system is as follows:

1) The highest level mechanism (blue box) consists of the basal ganglia and a portion of the cerebral cortex. According to the Brodmann partition [31], this mechanism mainly includes

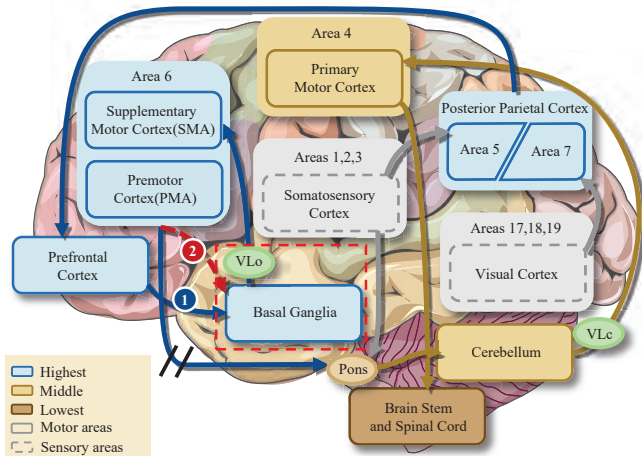


Fig. 1. The central motor system mechanism, with three colors representing different levels of the motor system, and sensory and motor regions distinguished by dashed and solid lines. The red dashed box displays two functions of the basal ganglia. ① represents its decision-making function, while ② represents the motor activity regulating function of the basal ganglia.

the posterior parietal cortex (areas 5 and 7) and prefrontal cortex, basal ganglia, as well as the supplementary motor area (SMA) and premotor cortex (PMA) located in area 6. Firstly, areas 5 and 7 of the parietal cortex serve as the input parts of the highest level structure, responsible for processing proprioceptive information from the somatosensory cortex (areas 1, 2, and 3) and external information from the visual cortex (areas 17, 18, and 19), respectively. The prefrontal cortex is connected to the posterior parietal cortex and is responsible for further processing information from the parietal lobe. Subsequently, the basal ganglia processes information from the prefrontal cortex (basal ganglia function ①), and through its internal regulatory processes, transmits the results to the oral part of the thalamic ventral lateral nucleus (VLo), and then to the cortical area 6, especially SMA. Then SMA and PMA participate in motor planning together [32] and send control signals to the next level control mechanism.

2) The middle level mechanism (yellow box) is mainly composed of the pons, cerebellum, and the primary motor cortex located in cortical area 4. The proprioceptive information from the somatosensory cortex and the control signals from the cortical area 6 pass through the pontine nucleus in the pons, transmit to the cerebellum, and finally project to the primary motor cortex through the caudal part of the thalamic ventral lateral nucleus (VLc). But even if the connection between the cortical area 6 and cerebellum is severed (as shown by the black double slash in Fig.1), the cerebellum can still make decisions based solely on proprioceptive information. Therefore, the cerebellum has its own learning circuit. It needs to learn how to accept different skill signals from the higher level and switch between various motor patterns with different levels of activity (basal ganglia function ②), as well as how to maintain basic motor ability in the absence of guidance skill signals.

3) Ultimately, the primary motor cortex transmits these basic control signals to the lowest level executing mechanisms

(brown box), including the brain stem and spinal cord, thereby mobilizing muscle cells to enable animals to complete complex movements.

As another important mechanism in the process of motor control, the basal ganglia plays two important roles (Arrows indicated by two serial numbers in Fig.1):

- ①) Decision making function: participate in motor decision-making and information dimensionality reduction with cortical regions. And select skill instructions with appropriate activity levels to achieve motor goals [14] [33].
- ②) Motor activity regulating function: decode the skill instructions output by the cortical area 6 to the cerebellum, then perform activity calculation and allocation. Researches have shown that the basal ganglia promote and inhibit motor activity through direct and indirect pathways formed internally [33] [34] [35] [36].

B. CMSRL Algorithm Overview

Based on the analysis results of CMS, we integrate these mechanisms into unsupervised pre-training RL, propose the CMSRL algorithm and use the Mujoco physics engine [37] to build a simulation environment.

The overall structure of the algorithm is shown in Fig.2. The actuators of the simulation engine are used to replace the lowest level mechanisms, while the sensors are used to simulate the sensory areas of cortex. The middle and the highest levels mechanisms of the CMS correspond to the low-level and high-level policies of the algorithm, respectively.

The training process includes two stages: pre-training and task-training. In the pre-training stage, skill z is sampled from a random discrete skill space $\mathcal{Z} = \{z_i\}$. Then it is encoded into a latent space of the d_z dimension and serves as input z^c for the low-level policy $\pi(a|s, z^c)$. Unlike most previous unsupervised reinforcement learning techniques [19] [20] [21], we do not directly use the skill of random encoding. Instead, we introduce skill diversity objective (SD) in the encoding process, so that different skills can be evenly distributed in the latent space, in order to increase the diversity of different behaviors. In addition, we design a decoder and skill activity calculation function $h(\hat{z})$ to assign activity values to each skill. By combining mutual information rewards and designed basic motor rewards, the low-level policy can acquire basic motor abilities and response functions to different skills. Then, during the task-training phase, the high-level policy $\psi(z^c|s_t, s_t^e)$ obtains robot states s_t and environmental information s_t^e to provide guiding skills, enabling the low-level policy to execute new tasks.

C. Skill Encoder

The discrete skill space \mathcal{Z} consists of C different skills, $\mathcal{Z} = \{z_0, z_1, \dots, z_i, \dots, z_{C-1}\}$. We use a uniform distribution $p(z) = U(0, C-1)$ to sample skills. Through the one-hot encoding format, the discrete skill z_i is first converted into a C -dimensional vector $v_i(j) = \delta_{ij}(z_i)$, where δ is the kronecker delta function (if $i = j$, $\delta_{ij} = 1$, else $\delta_{ij} = 0$). To map arbitrary one-hot skill v to the latent space \mathcal{Z}^c of the d_z

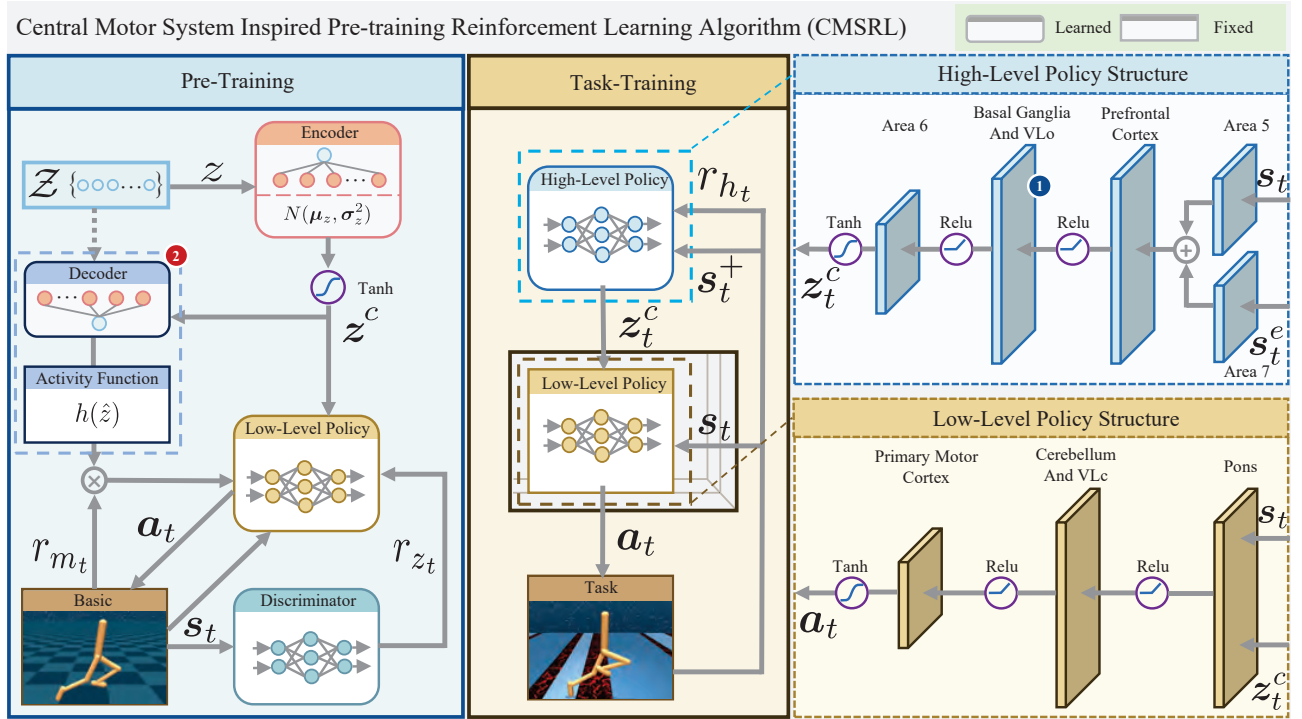


Fig. 2. The CMSRL algorithm is divided into two parts: in the pre-training phase, a low-level policy is obtained, which is responsible for receiving signals from the basal ganglia and adjusting the robot's willingness to move and posture. Through task-training, a high-level policy is obtained, which is responsible for processing external environmental information and generating skill signals suitable for task solving.

dimension, we use a parameterized encoder E_{ξ} . The latent skill z^c is generated by the following equation

$$z^c \sim \mathcal{N}(\mu_z, \sigma_z^2), \quad (7)$$

where \mathcal{N} is a normal distribution, $\mu_z = E_{\xi}(v)$, σ_z is the fixed standard deviation. By this way, the encoded skills will be centered around $E_{\xi}(v)$ and dispersed into skill clusters, which is beneficial for enhancing the fault tolerance of the low-level policy. To ensure the sampling efficiency, bounded latent space is used, where z^c can be limited to $[-1, 1]$ through the processing of tanh function.

To increase the gap between different latent skills, we update E_{ξ} by maximizing the L2-norm between continuous skill vectors, which is called the skill diversity objective, as shown in the following equation

$$\max_{\xi} L(\xi) = \sum_{i=0}^{C-2} \sum_{j=i+1}^{C-1} \|\hat{\mu}_{z_i} - \hat{\mu}_{z_j}\|_2, \quad (8)$$

where $\hat{\mu}_z = \frac{\tanh(\mu_z)}{\|\mu_z\|_2}$.

D. Decoder and Skill Activity Calculation Function

The motor activity regulatory of the basal ganglia is mainly achieved through the antagonistic effects of two neurotransmitters (GLu, GABA) and two internal pathways (as shown in Fig.3). The skill information from SMA/PMA is first decoded by Striatum. Subsequently, it passes through both direct and indirect pathways, ultimately affecting the GLu concentration output from VL0.

The direct pathway (striatum \rightarrow GPI/SNr \rightarrow Thalamus (VL0)) promotes the production of movement. The inhibitory neurotransmitter GABA inhibits GPI, resulting in Thalamus producing more excitatory neurotransmitter GLu, which in turn makes the cerebral cortex more active. On the contrary, the indirect pathway (striatum \rightarrow GPe \rightarrow STN \rightarrow Thalamus (VL0)) inhibit the production of movement. In addition, the SNc exerts opposite effects on the D1 and D2 receptors in the striatum by releasing dopamine (DA). The activation of D1 receptors enhances the direct pathway, while the activation of D2 receptors inhibits the indirect pathway. Therefore, DA overall enhances the activity of the cortex.

Lesions in the basal ganglia can lead to Huntington's disease (HD) [38] or Parkinson's disease (PD) [39]. Due to genetic defects, HD patients experience uncontrolled dance symptoms due to indirect pathway blockage. However, PD patients experience inhibition of dopamine secretion due to SNc cell apoptosis, making it difficult for them to engage in voluntary movements.

Inspired by the internal mechanism of basal ganglia motor activity regulation (basal ganglia function ②), we design the skill decoder and skill activity calculation function.

1) We use a parameterized decoder D_{ζ} to process the latent skill z^c and provide a predicted value \hat{z} , as shown in the following equation

$$\hat{z} = \arg \max_i D_{\zeta}(z^c). \quad (9)$$

The optimization objective of the decoder D_{ζ} is shown in

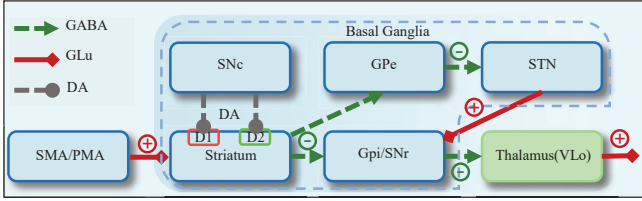


Fig. 3. The internal physiological structure diagram of the basal ganglia. The three different neurotransmitters in the figure are represented by different line segments. Positive and negative symbols are used to indicate the promoting and inhibitory effects of neurotransmitters on neurons.

the following equation

$$\min_{\zeta} L(\zeta) = \frac{1}{C} \sum_{i=0}^C \|v_i - \hat{v}_i\|^2, \quad (10)$$

where v_i refers to the one-hot encoding vector corresponding to the real skill z , $\hat{v}_i = D_{\zeta}(z_i^c)$.

2) Based on the internal antagonistic effect of the basal ganglia, we design a skill activity calculation function $h(\hat{z})$

$$\begin{aligned} h(\hat{z}) &= \min \left[H \left(\exp(D) \frac{k_1}{k_2} \hat{z} - \exp(-D) \frac{k_1}{k_2} \hat{z} \right), 1 \right] \\ &= \min \left[H \frac{k_1 (\exp(2D) - 1)}{k_2 \exp(D)} \hat{z}, 1 \right], \end{aligned} \quad (11)$$

where $D \in [0, 1]$ represents dopamine concentration, $k_1 \in (0, 1]$ and $k_2 \in (0, 1]$ respectively represent the degree of activation of direct and indirect pathways, H is the normalization constant, $H = \exp(1) / [(C - 1)(\exp(2) - 1)]$.

By doing so, the function can reflect the internal activity mechanism of the basal ganglia. Under the normal condition, $D = 1$, and the activation ratio of the two pathways $k_1/k_2 = 1$. At this point, the activity calculation function result is shown in the light blue line in Fig.4, where each skill corresponds uniformly to a GLu concentration between 0 and 1. For PD patients, dopamine secretion is insufficient, with $D < 1$, resulting in a decrease in the slope of the curve, as shown by dots and square lines. For HD patients, due to the inability to activate the indirect pathway, $k_1/k_2 > 1$. Therefore, the entire curve will be raised to an abnormal slope, resulting in each skill corresponding to a high GLu concentration. The impact of these anomalies on motor abilities will be experimentally analyzed in Section V-C.

The pseudo code of training the encoder and decoder is shown in Algorithm 1.

E. Mixed Reward for Pre-training RL

Inspired by the regulatory function of the cerebellum on basic motor and balance abilities, we designed a basic motor reward r_{m_t} to quantify the basic motor abilities produced by the cerebellum.

$$r_{m_t}(\mathbf{s}_t, \mathbf{a}_t) = w_v \mathbf{v}_x - w_c \|\mathbf{a}_t\|^2 + w_f I[\mathbf{s}_t \notin \bar{\mathbf{s}}_t], \quad (12)$$

where w_v is the weight of torso velocity, \mathbf{v}_x represents the velocity in the x-axis, w_f is the weight of balance ability, w_c is the weight of energy consumption, $I[\cdot]$ is the indicator function, $\bar{\mathbf{s}}$ is the invalid state after a fall.

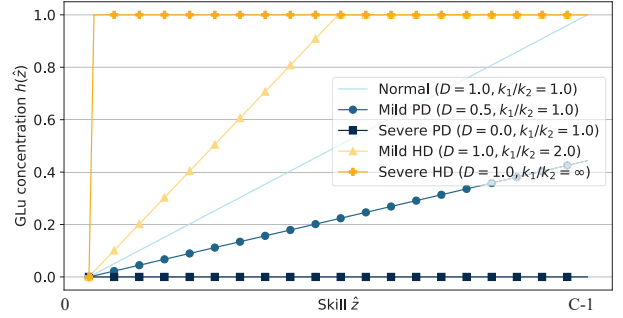


Fig. 4. The impact of internal parameter changes on the skill activity calculation equation.

Algorithm 1 Encoder Decoder pseudo code

- 1: **Input:** discrete skills number C ; maximum number of episodes N_1 ; standard deviation σ_z ; learning rates η_{ξ} , η_{ζ} for ξ , ζ .
- 2: **Output:** optimal parameters ξ^* for Encoder; optimal parameters ζ^* for Decoder;
- 3: **Init:** $E_{\xi} \leftarrow$ Encoder; $D_{\zeta} \leftarrow$ Decoder; $\mathcal{D} \leftarrow$ Dataset;
- 4: **for** $j \leftarrow 1, N_1$ **do**
- 5: **for** $i \leftarrow 0, C - 1$ **do**
- 6: Get $z_i = i$
- 7: Compute one-hot vector $\mathbf{v}_i = \delta_{ij}(z_i)$
- 8: $\mu_{z_i} = E_{\xi}(\mathbf{v}_i)$
- 9: Sample latent skill $z_i^c \sim \mathcal{N}(\mu_{z_i}, \sigma_z^2)$
- 10: $z_i^c \leftarrow \tanh(z_i^c)$
- 11: $\hat{v}_i = D_{\zeta}(z_i^c)$
- 12: Store $(\mathbf{v}_i, \hat{v}_i, \mu_{z_i}, z_i^c)$ in \mathcal{D}
- 13: **end for**
- 14: Use \mathcal{D} and Adam to update ξ by Equation (8)
- 15: Use \mathcal{D} and Adam to update ζ by Equation (10)
- 16: **end for**

In order to generate different robot motor patterns for different skills, we use mutual information as another reward $r_{z_t}(\mathbf{s}_t, \mathbf{z}^c)$

$$r_{z_t}(\mathbf{s}_t, \mathbf{z}^c) = -\log p(\mathbf{z}^c) + \log q_{\varphi}(\phi(\mathbf{s}_{t+1})), \quad (13)$$

where $q_{\varphi} : \mathcal{S} \rightarrow \mathcal{Z}$ is a parameterized variational estimation discriminator, and ϕ is a feature extraction function, \hat{z} is the decoded skill of z^c calculated using Equation (9).

The variational estimation parameters φ can be updated by the following equation

$$\min_{\varphi} L(\varphi) = -\frac{1}{B} \sum_{j=1}^B \sum_{i=0}^{C-1} \hat{v}_{j_i} \log q_{\varphi}(\phi(\mathbf{s}_j)), \quad (14)$$

where \hat{v}_j is the one-hot vector of \hat{z}_j .

Based on the basic motor function of the cerebellum and the motor regulation function of the basal ganglia, we propose a mixed reward function as shown below

$$r_{mix_t}(\mathbf{s}_t, \mathbf{a}_t, \mathbf{z}^c) = \beta r_{z_t}(\mathbf{s}_t, \mathbf{z}^c) + (1 - \beta) h(\hat{z}) r_{m_t}(\mathbf{s}_t, \mathbf{a}_t), \quad (15)$$

where $\beta \in (0, 1)$ is the proportion of reward.

According to the definition of RL, the following equation can be used to describe the optimization objective of pre-training

$$\max_{\pi} \mathbb{E}_{p(\mathbf{z}^c)} \mathbb{E}_{p(\tau|\pi, \mathbf{z}^c)} \left[\sum_{t=0}^{T-1} \gamma^t r_{mix_t}(\mathbf{s}_t, \mathbf{a}_t, \mathbf{z}^c) \right], \quad (16)$$

which can be optimized using the Soft Actor-Critic [40]. For a fixed $\pi(\mathbf{a}|\mathbf{s}, \mathbf{z}^c)$, the soft Q-value $Q : \mathcal{S} \times \mathcal{A} \times \mathcal{Z}^c$ can be written as

$$Q(\mathbf{s}_t, \mathbf{a}_t, \mathbf{z}^c) = r_{mix_t}(\mathbf{s}_t, \mathbf{a}_t, \mathbf{z}^c) + \gamma V(\mathbf{s}_{t+1}), \quad (17)$$

where

$$V(\mathbf{s}_t) = \mathbb{E}_{\mathbf{a}_t \sim \pi(\cdot|\mathbf{s}_t, \mathbf{z}^c)} [Q(\mathbf{s}_t, \mathbf{a}_t, \mathbf{z}^c) - \alpha \log \pi(\mathbf{a}_t|\mathbf{s}_t, \mathbf{z}^c)]. \quad (18)$$

We use parameterized soft Q-value function $Q_{\rho}(\mathbf{s}_t, \mathbf{a}_t, \mathbf{z}^c)$ and policy $\pi_{\theta}(\mathbf{a}_t|\mathbf{s}_t, \mathbf{z}^c)$, with neural network parameters of ρ and θ , respectively. The structure of the policy network is shown in the bottom right corner of Fig.2. The parameters ρ of Q-function can be trained using the following equation

$$\min_{\rho} J(\rho) = \mathbb{E}_{(\mathbf{s}_t, \mathbf{a}_t, \mathbf{z}^c) \sim \mathcal{B}} \left[\frac{1}{2} (Q_{\rho}(\mathbf{s}_t, \mathbf{a}_t, \mathbf{z}^c) - G)^2 \right], \quad (19)$$

where $G = r_{mix_t}(\mathbf{s}_t, \mathbf{a}_t, \mathbf{z}^c) + \gamma V_{\bar{\rho}}(\mathbf{s}_{t+1})$, the value function is parameterized through the parameters ρ via Equation (18). The update process uses target parameters $\bar{\rho}$, which can enhance the stability of training. While the policy parameters can be learned through the following equation

$$\begin{aligned} \min_{\theta} J(\theta) = \\ \mathbb{E}_{(\mathbf{s}_t, \mathbf{z}^c) \sim \mathcal{B}} [\mathbb{E}_{\mathbf{a}_t \sim \pi_{\theta}} [\alpha \log \pi_{\theta}(\mathbf{a}_t|\mathbf{s}_t, \mathbf{z}^c) - Q_{\rho}(\mathbf{s}_t, \mathbf{a}_t, \mathbf{z}^c)]]. \end{aligned} \quad (20)$$

In summary, Algorithm 2 provides the pseudo code for the pre-training process.

F. Task-training

After obtaining the low-level policy $\pi_{\theta^*}(\mathbf{a}|\mathbf{s}, \mathbf{z}^c)$, the low-dimensional continuous skill space \mathcal{Z}^c can be used to learn the high-level policy $\psi(\mathbf{z}^c|\mathbf{s}, \mathbf{s}^e)$. In order to maintain the consistency of the reward function in different tasks, sparse rewards r_{h_t} are used in the task environment, and robots only receive positive rewards when completing a specified goal. Therefore, in this environment, robots need to have strong exploration ability to complete tasks.

According to the characteristics of the CMS, the high-level policy has strict temporal abstraction, which means switching skill actions \mathbf{z}_{c_t} every k time steps, while the low-level policy generates different basic actions \mathbf{a}_t each time step. This temporal abstraction can lead to a decrease in the training efficiency of the high-level policy, as only T/k transitions can be obtained within the T time step. Therefore, we adopt a step conditioned critical structure as described in [8] [41]. By using this architecture, we can obtain $T - (k - 1)$ transformed data within T time steps to increase the number of samples and ensure training efficiency under the constraints of time abstraction.

Algorithm 2 Pre-training pseudo code

- 1: **Input:** maximum number of episodes N_2 ; maximum number of time-step T ; discount factor γ ; proportion of reward β ; batch size B ; discrete skills number C ; number of update episodes n ; learning rates $\eta_{\varphi}, \eta_{\theta}, \eta_{\rho}$ for φ, θ, ρ .
 - 2: **Output:** optimal parameters θ^* for the low-level policy;
 - 3: **Init:** $\pi_{\theta} \leftarrow$ low-level policy; $E_{\xi^*} \leftarrow$ Encoder; $D_{\zeta^*} \leftarrow$ Decoder; $q_{\varphi} \leftarrow$ discriminator; $Q_{\rho} \leftarrow$ Q-function; $\mathcal{B} \leftarrow$ Buffer;
 - 4: **for** $i \leftarrow 1, N_2$ **do**
 - 5: Sample skill $z \sim p(z) = U(0, C - 1)$
 - 6: Get one-hot vector $\mathbf{v} = \delta_{i,j}(z)$
 - 7: $done = \text{False}$
 - 8: **for** time-step $t = 0, \dots, T - 1$ **do**
 - 9: Get latent skill $\mathbf{z}^c \sim N(E_{\xi^*}(\mathbf{v}), \sigma_z^2)$
 - 10: $\mathbf{z}^c \leftarrow \tanh(\mathbf{z}^c)$
 - 11: $\hat{z} = \arg \max_i D_{\zeta^*}(\mathbf{z}^c)$
 - 12: Sample action $\mathbf{a}_t \sim \pi_{\theta}(\mathbf{a}_t|\mathbf{s}_t, \mathbf{z}^c)$
 - 13: $\mathbf{s}_{t+1}, r_{m_t}, done \sim p(\mathbf{s}_{t+1}|\mathbf{s}_t, \mathbf{a}_t)$
 - 14: Compute r_{mix_t} according to Equation (15)
 - 15: Store $(\mathbf{s}_t, \mathbf{s}_{t+1}, \mathbf{a}_t, \mathbf{z}^c, \hat{z}, r_{mix_t})$ in \mathcal{B}
 - 16: $\mathbf{s}_t \leftarrow \mathbf{s}_{t+1}$
 - 17: **if** $done$ **then**
 - 18: $break$
 - 19: **end if**
 - 20: **end for**
 - 21: **for** update-step $u = 1, \dots, n$ **do**
 - 22: $b_B \sim \mathcal{B}$
 - 23: Update φ using Adam according to Equation (14)
 - 24: Update ρ using Adam according to Equation (19)
 - 25: Update θ using Adam according to Equation (20)
 - 26: **end for**
 - 27: **end for**
-

Due to the use of step-conditioned critic, some improvements need to be made to the Q-value function $Q(\mathbf{s}, \mathbf{s}^e, \mathbf{z}^c)$ and its optimization objectives. To simplify calculations, $\mathbf{s}_t, \mathbf{s}_t^e$ are denoted as \mathbf{s}_t^+ together. The improved Q-value function adds input $i = t \bmod k (0 \leq i < k)$ to record the number of executed steps for \mathbf{z}_t^c . The improved Q-value function is shown as follow

$$Q(\mathbf{s}_t^+, \mathbf{z}_t^c, i) = \left(\sum_{j=0}^{k-i-1} \gamma^j r_{h_{t+j}} \right) + \gamma^{k-i} V(\mathbf{s}_{t+k-i}^+), \quad (21)$$

where

$$V(\mathbf{s}_t^+) = \mathbb{E}_{\mathbf{z}_t^c \sim \psi} [Q(\mathbf{s}_t^+, \mathbf{z}_t^c, 0) - \alpha \log \psi(\mathbf{z}_t^c|\mathbf{s}_t^+)]. \quad (22)$$

Similarly, we use parameterized soft Q-value function $Q_{\mathbf{v}}(\mathbf{s}_t^+, \mathbf{z}_t^c, i)$ and policy $\psi_{\omega}(\mathbf{z}^c|\mathbf{s}_t^+)$, with neural network parameters of \mathbf{v} and ω , respectively. The structure of the policy network is shown in the upper right corner of Fig.2, the decision-making function of the basal ganglia (basal ganglia function ①) is modeled as a layer of neural network. The

parameters \mathbf{v} of Q-function can be trained using the following equation

$$\min_{\mathbf{v}} J(\mathbf{v}) = \mathbb{E}_{(\mathbf{s}_{t,\dots,t+k-1}, \mathbf{z}_t^c, i) \sim \mathcal{B}} \left[\frac{1}{2} \left(Q_{\mathbf{v}}(\mathbf{s}_t^+, \mathbf{z}_t^c, i) - G' \right)^2 \right], \quad (23)$$

where $G' = \sum_{j=0}^{k-i-1} (\gamma^j r_{h_{t+j}}) + \gamma^{k-i} V(\mathbf{s}_{t+k-i}^+)$. And the optimization target for the high-level policy parameters ω is shown in the following equation

$$\min_{\omega} J(\omega) = \mathbb{E}_{\mathbf{s}_t^+ \sim \mathcal{B}} \left[\mathbb{E}_{\mathbf{z}_t^c \sim \psi_{\omega}} \left[\alpha \log \psi_{\omega}(\mathbf{z}_t^c | \mathbf{s}_t^+) - Q_{\mathbf{v}}(\mathbf{s}_t^+, \mathbf{z}_t^c, 0) \right] \right]. \quad (24)$$

Algorithm 3 provides the pseudo code for the task-training process. In the pseudo code, the parameters of the low-level policy are initialized by θ^* obtained from Algorithm 2.

Algorithm 3 Task-training pseudo code

```

1: Input: maximum number of episodes  $N_3$ ; maximum
   number of time-step  $T$ ; discount factor  $\gamma$ ; batch size  $B$ ;
   number of update episodes  $n$ ; high action interval  $k$ ;
   learning rates  $\eta_v, \eta_{\omega}$  for  $\mathbf{v}, \omega$ .
2: Output: optimal parameters  $\omega^*$  for high-level policy;
3: Init:  $\pi_{\theta^*} \leftarrow$  learned low-level policy;  $Q_{\mathbf{v}} \leftarrow$  Q-function;
    $\psi_{\omega} \leftarrow$  high-level policy;  $\mathcal{B} \leftarrow$  Buffer;
4: for  $i \leftarrow 1, N_3$  do
5:    $done = False$ 
6:   for time-step  $t = 0, \dots, T - 1$  do
7:     Compute  $i = (t \bmod k)$ 
8:     if  $i == 0$  then
9:       Sample high-action  $\mathbf{z}_t^c \sim \psi_{\omega}(\mathbf{z}_t^c | \mathbf{s}_t, \mathbf{s}_t^e)$ 
10:    end if
11:    Sample action  $\mathbf{a}_t \sim \pi_{\theta^*}(\mathbf{a}_t | \mathbf{s}_t, \mathbf{z}_t^c)$ 
12:     $\mathbf{s}_{t+1}, \mathbf{s}_{t+1}^e, r_{h_t}, done \sim p(\mathbf{s}_{t+1}, \mathbf{s}_{t+1}^e | \mathbf{s}_t, \mathbf{s}_t^e, \mathbf{a}_t)$ 
13:    Store  $(\mathbf{s}_t, \mathbf{s}_{t+1}, \mathbf{s}_t^e, \mathbf{s}_{t+1}^e, \mathbf{z}_t^c, r_{h_t}, i)$  in  $\mathcal{B}$ 
14:     $\mathbf{s}_t, \mathbf{s}_t^e \leftarrow \mathbf{s}_{t+1}, \mathbf{s}_{t+1}^e$ 
15:    if  $done$  then
16:       $break$ 
17:    end if
18:  end for
19:  for update-step  $u = 1, \dots, n$  do
20:     $b_B \sim \mathcal{B}$ 
21:    Update  $\mathbf{v}$  using Adam according to Equation (23)
22:    Update  $\omega$  using Adam according to Equation (24)
23:  end for
24: end for

```

V. EXPERIMENT

Our experiments aims to explore the following questions.

- 1) Does the low-level policy possess decision-making abilities similar to those of the cerebellum ?
- 2) What is the impact on the robot's motor ability when the skill activity calculation function is abnormal ?
- 3) What is the impact of the proposed new skill encoding method and mixed rewards on the performance of robots in task environments ?

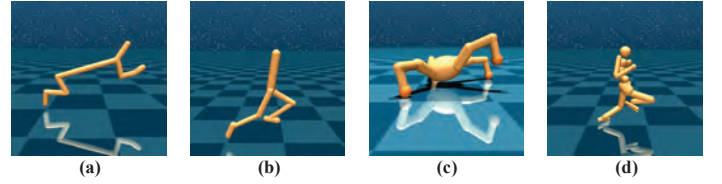


Fig. 5. Different types of robots in simulation environments. (a) ‘‘Cheetah’’. (b) ‘‘Walker’’. (c) ‘‘Quadruped’’. (d) ‘‘Humanoid’’.

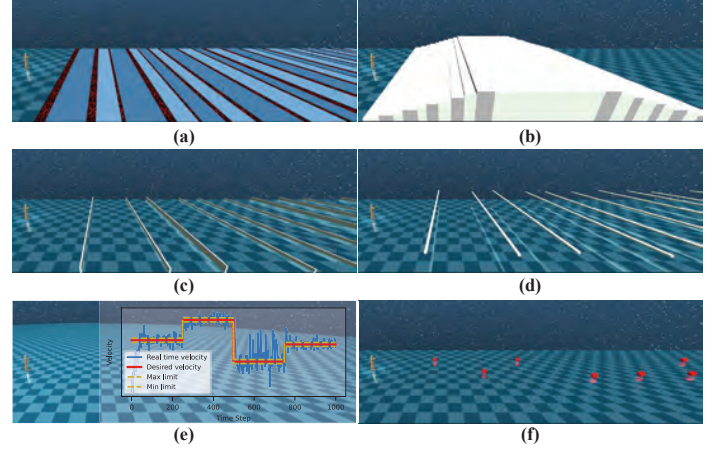


Fig. 6. Different task environments. (a) ‘‘Gaps’’: The robot needs to constantly move forward and cross the magma, but once the robot comes into contact with the magma or falls, the task ends. (b) ‘‘Stairs’’: The robot needs to cross the steps of ascent and descent. (c) ‘‘Hurdles’’: The robot needs to adjust its posture to cross the hurdles. (d) ‘‘Limbos’’: The robot needs to lower its center of gravity during movement to pass through the interceptor. (e) ‘‘V-track’’: The robot needs to track four random expected speeds and maintain its own speed within a specified deviation range from the expected speed. (f) ‘‘Goals’’: The robot needs to touch more target points within a limited time.

- 4) Has the proposed method made progress in various robot and task environments compared to the state-of-the-art RL algorithms ?

A. Experimental Setup

To explore the above issues, we use the Mujoco simulation engine [37] to design six challenging motor control environments for four different types of robots, and conduct experiments in these environments. The types of robots are shown in Fig.5, including ‘‘Cheetah’’, ‘‘Walker’’, ‘‘Quadruped’’, ‘‘Humanoid’’. The first two types of robots are low degree of freedom robots in two-dimensional space, while the latter two are high degree of freedom robots in three-dimensional space.

The environments are divided into two types: basic environment and task environment. The basic environment is used to train and test the low-level policy, while the task environment is used to train the high-level policy and test the overall performance of algorithms. It should be pointed out that during the pre-training period, we preprocess the states of the ‘‘Quadruped’’ and ‘‘Humanoid’’ robots using the function ϕ to calculate the mutual information reward r_z . For ‘‘Quadruped’’, we use the swing decomposition method to calculate the rotation angles of x, y, and z from the global direction of the torso. In addition, we also calculate the distances of the

TABLE I
HYPER-PARAMETERS FOR PRE-TRAINING

Parameter	Value
Episodes number N_1	$1 \cdot 10^5$
Episodes number N_2	$2 \cdot 10^5$
Batch size B	256
Horizon T	100
Update numbers n	50
Number of skills C	10
Latent skill dim d_z	7
Torso velocity weight w_v	1.0
Balance ability weight w_f	0.1
Energy consumption weight w_c	0.1
Proportion of reward β	0.5
Dopamine concentration D	1.0
Degree of activation of direct pathway k_1	1.0
Degree of activation of indirect pathway k_2	1.0
Std of skill coding σ_z	0.3
Learning rates $\eta_{(\cdot)}$	$3 \cdot 10^{-4}$
Discount factor γ	0.99
Target network update factor $\bar{\tau}$	0.01

TABLE II
HYPER-PARAMETERS FOR TASK-TRAINING

Parameter	Value
Episodes number N_3	$1 \cdot 10^4$
Batch size B	256
Horizon T	1000
Update numbers n	50
Learning rates $\eta_{(\cdot)}$	$3 \cdot 10^{-4}$
Discount factor γ	0.99
Target network update factor $\bar{\tau}$	0.005
Action interval k	3

four toes relative to the torso in the x, y, and z directions and use the above information as the preprocessed state $\phi(s)$. As for “Humanoid”, we adopt a similar approach to the former, but replace the relative distances with the positions of the remaining parts of the robot relative to the pelvis in the x, y, and z directions.

The task environment mainly designed based on the Bisk suite [8]. The tasks “Gaps”, “Stairs”, “Hurdles”, and “Limbos” remain unchanged. However, “Cheetah” and “Quadruped” robots are added to these tasks. And we design two new tasks, “V-track” and “Goals”, all tasks are shown in Fig.6. The reward function r_h for all tasks is in discrete form. When the robot meets the target requirements, it will receive a reward value of +1, while when the robot enters an invalid state, it will receive a reward of -1 and the task will terminate. Under other conditions, the reward is 0. The hyperparameters used in the encoder decoder and pre-training process are shown in Table I, while the hyperparameters used in the task-training process are shown in Table II.

B. Evaluation of the Low-level Policy

The pre-training process continues until the return of the mixed reward r_{mix} converges. Fig.7 shows the mean and standard deviations of fusion rewards for different robots in each iteration. The means and variances are calculated over three learning sessions of 20 million samples each. The

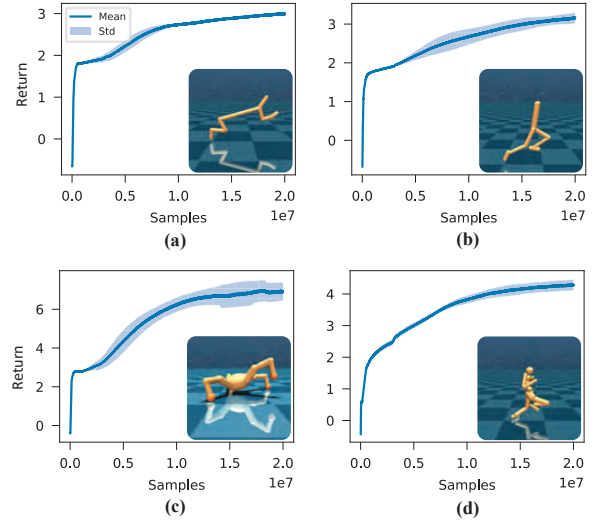


Fig. 7. The r_{mix} return images of the four robots over time during the pre-training process. The curve represents the average value obtained from 3 sets of random experiments, and the shaded portion represents the standard deviation. (a)“Cheetah”. (b).“Walker”. (c)“Quadruped”. (d).“Humanoid”.

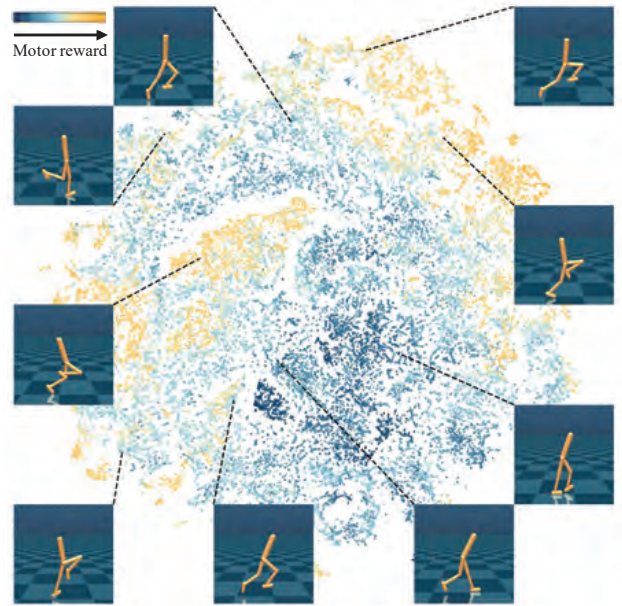


Fig. 8. The state-skill pairs t-sne scatter plot obtained by the low-level policy of the “Walker” robot under the action of random skills from the \mathcal{Z}^c .

results show that all four robots achieved convergence of the rewards in pre-training. To answer question 1), we need to determine whether the low-level policy possesses the following properties:

- Can low-level policy make actions with different motor patterns and levels of activity for different skill signals ?
- Can low-level policy still maintain basic movement ability of robots after skill signals are cut off ?

We first conduct a random skill input experiment using the trained low-level policy network in the basic environments. Randomly sample 200 skill z^c from the \mathcal{Z}^c space as skill inputs for the low-level policy. Under the influence of skills, robots interact with the environment and receive several motor

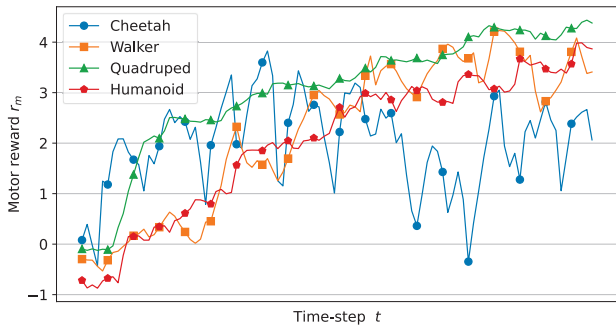


Fig. 9. The impact curve of the low-level policy on the motor ability of four types of robots without skill signal input.

rewards r_m . Using the r_m value as a measure of motor activity, we use the t-sne [42] dimensionality reduction method to transform the input (s_t, z^c) of the policy network into a two-dimensional vector. Fig.8 shows the t-sne scatter image of the “Walker” robot, each scatter in the figure represents a state-skill pair (s_t, z^c) , and the color of the scatter represents r_m . The image connected to the scatter shows the robot’s posture corresponding to this skill. From the graph, it can be seen that different random skills can make the robot exhibit uniform motor activity from low to high, and each skill corresponds to a different motor pattern. The scattered images of other robots exhibit similar patterns, these results demonstrate that the low-level policy has the property a).

To demonstrate the autonomy of the low-level policy, we set the skill input of the policy network to 0 to simulate the situation where the skill signal is cut off, and observe the motor pattern of the robot. Fig.9 shows the variation curves of 100 time step motor rewards for four types of robots under the condition of skill value $z^c = 0$. From the graph, it can be seen that even without skill information guidance, the low-level policy can still maintain the basic movement ability of robots, which proves the low-level policy has the property b).

Based on the results of the above two experiments, we can answer question 1) that the low-level policy possess decision-making abilities similar to those of the cerebellum.

C. The Impact of Abnormal Skill Activity Calculation Function on Motor Ability

Based on the motor regulation mechanism of the basal ganglia, we propose a skill activity calculation function as shown in Equation (11). By adjusting the dopamine concentration parameter D and the activation level parameters k_1 and k_2 of the two pathways, we can change the output GLU concentration.

The preliminary experiments have demonstrated that under normal parameter effects, the low-level policy can generate motor regulation abilities similar to those of the cerebellum, allowing for flexible responses to different skills. Here, we design an experiment to further analyze the impact of the skill activity calculation function with abnormal parameters on the low-level policy’s motor ability, in order to answer the question 2).

Corresponding to the several abnormal situations in Fig.4, we design several sets of parameters as shown in Table III. By using skill activity calculation functions with different parameters and through the pre-training process, corresponding low-level policies can be obtained. Similarly, randomly select 200 skills z^c from the \mathcal{Z}^c space as skill inputs for low-level policies. The robot interacts with the environment for 250 steps under each skill, and we can receive several motor rewards of r_m . The distribution of these rewards is shown in Fig10.

For HD individuals, the overall skill activity level is relatively high, so the motor reward r_m values are mainly distributed in the right range, and the robot exhibits uncontrollable motion states. On the contrary, for PD individuals, due to the impact of dopamine deficiency, the overall level of skill activity is lower than the normal level, which leads to r_m being concentrated in the left range. Due to this anomaly, it is difficult for the robot to initiate movement. Based on the above experimental results, abnormal skill activity calculation function can lead to behavior patterns similar to basal ganglia related diseases in robots.

TABLE III
PARAMETER TABLE FOR ABNORMAL SKILL ACTIVITY CALCULATION FUNCTION

Parameter	Sever HD	Mild HD	Normal	Mild PD	Sever PD
D	1.0	1.0	1.0	0.5	0.0
k_1	1.0	1.0	1.0	1.0	1.0
k_2	0.0	0.5	1.0	1.0	1.0

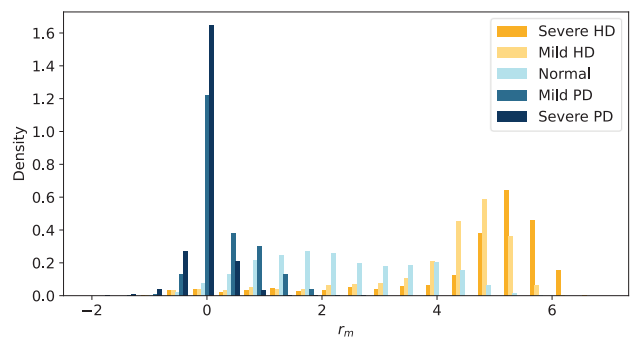


Fig. 10. The distribution of basic motor rewards r_m generated by the low-level policies of the “Walker” robot under different skill activity calculation functions.

D. Performance of CMSRL Algorithm in Task Environments

To answer question 3), we analyze the impact of various proposed mechanisms on algorithm performance. By designing ablation experiments, we compare the performance of the CMSRL algorithm with three scenarios: the absence of skill activity calculation function weighted motor rewards (No $h(\hat{z})r_m$), the absence of a new encoding method (No E-SD), and the simultaneous absence of both (No E-SD + No $h(\hat{z})r_m$).

To answer question 4), we also compare the CMSRL algorithm with the APS algorithm [21] to verify the effectiveness of the proposed pre-training method, where APS algorithm

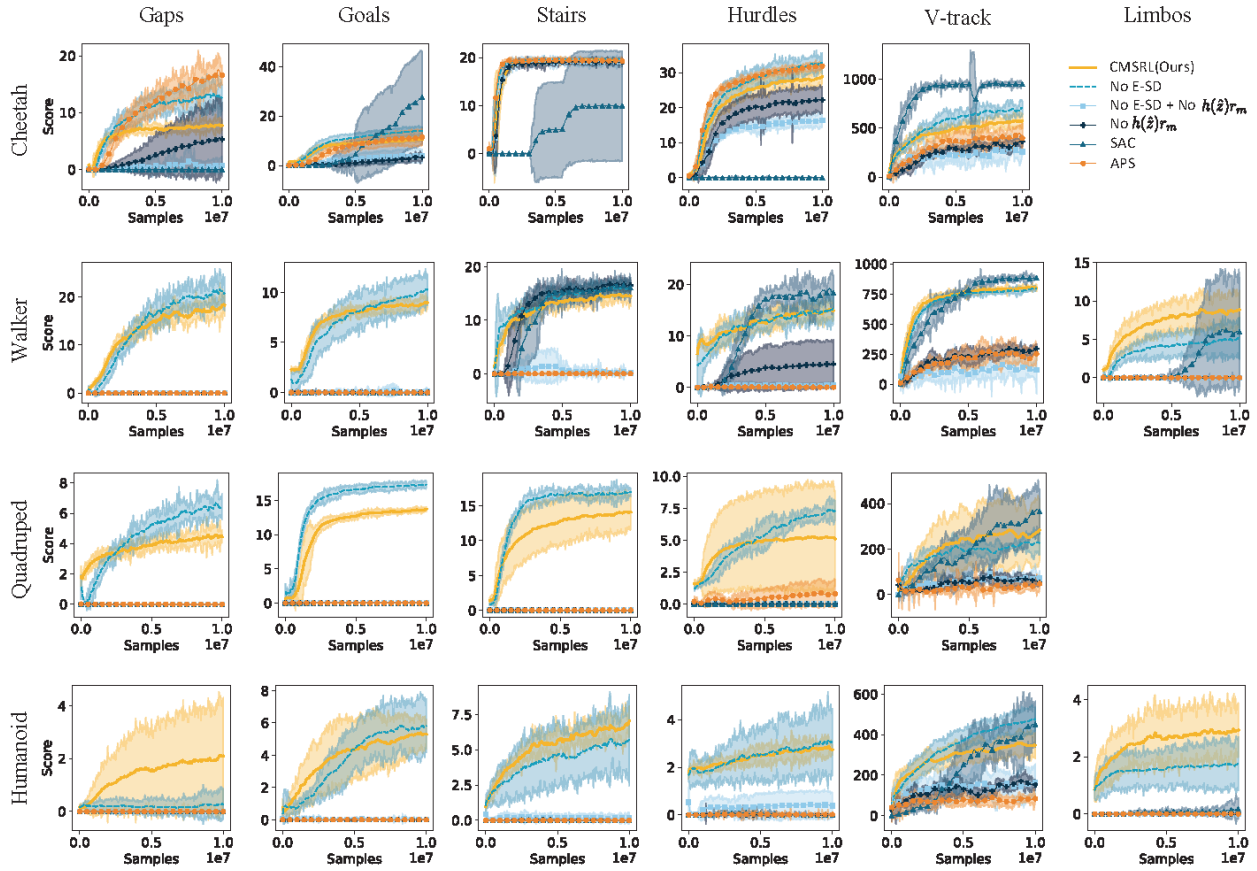


Fig. 11. Score curves of different algorithm training processes for four types of robots in 22 task environments. Including the APS algorithm, SAC algorithm and CMSRL algorithm under normal conditions, and three missing conditions. For each algorithm and task, four pairs of random seeds were used for multiple experiments (two sets of random seeds formed four combinations during pre-training and task-training). The single score in each experiment is the average score of 50 test environments. The line represents the average score of four parallel experiments, while the shaded area represents the standard deviation.

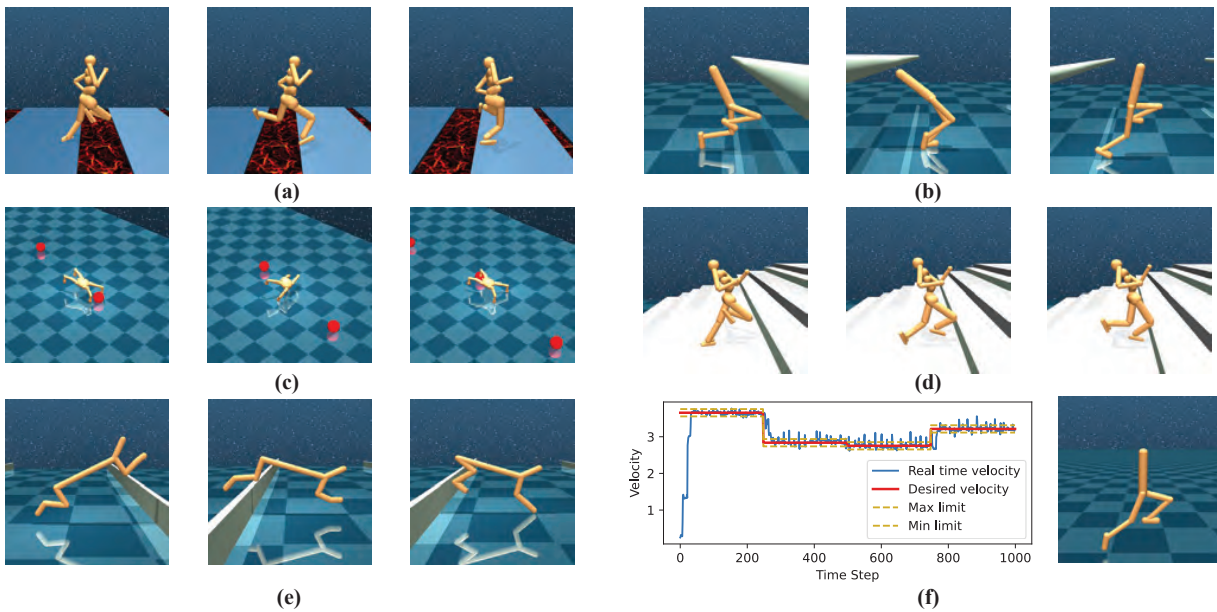


Fig. 12. The control performance of CMSRL algorithm in different robot task environments. (a) “Humanoid” robot in the “Gaps” task environment. (b) “Walker” robot in the “Limbos” task environment. (c) “Quadruped” robot in the “Goals” task environment. (e) “Humanoid” robot in the “Stairs” task environment. (f) “Cheetah” robot in the “Hurdles” task environment. (g) “Walker” robot in the “V-track” task environment.

is a state-of-the-art skill-based unsupervised reinforcement learning algorithm. On the other hand, we also compare the effectiveness of directly using the SAC algorithm to explore the advantages of hierarchical mechanisms.

Fig.11 shows the score curves of four types of robots in various task environments under different circumstances. During the training process, the robots were evaluated 50 times for every 50,000 sample points sampled, and their average evaluation value is recorded as the score. The broken line and shaded area represent the mean and variance of scores calculated in four experiments, with 10 million samples sampled in each experiment.

In the simplest “Cheetah” robot task environment, the models obtained under three missing conditions show comparable performance to the CMSRL algorithm. But as the difficulty of robot control increases, the “No $h(\hat{z})r_m$ ” and “No E-SD + No $h(\hat{z})r_m$ ” model cannot continue to produce meaningful results. This proves that the mixed rewards with skill activity calculation function weighted motor reward can improve the robot’s ability to apply skills in task environments. The “No E-SD” model performs similarly to CMSRL in different task environments, and even slightly better than CMSRL in low dimensional robot environments, but in the most complex “Humanoid” environment, the lack of diversity targets can lead to robots being unable to complete tasks that span gaps. This situation indicates that the proposed new skill encoding method can enable robots with more joints to perform better in more complex environments.

The APS algorithm and the SAC algorithm only demonstrate control effectiveness in some tasks of the two types of planar robots, but the CMSRL algorithm show robust control performance in all robot tasks. For example, Fig.12a shows the motor ability of the “Humanoid” robot in the “Gaps” task environment. Driven by the CMSRL algorithm, the robot exhibits jumping behavior that allows it to freely cross magma. From Fig.12b, it can be seen that the “Walker” robot will naturally change its posture when encountering obstacles higher than its own body. Fig.12c shows the target tracking skill of the “Quadruped” robot in the “Goals” task. Fig.12d shows the ability of the “Humanoid” robot to climb stairs. Fig.12e depicts the hurdle-crossing ability evolved by the “Cheetah” robot in the “Hurdles” task. Finally, Fig.12f shows the speed adjustment function of the “Walker” robot. These results demonstrate that CMSRL has made significant progress in robot task control. And it has been proven that the introduction of CMS architecture into the pre-training RL is effective, and the hierarchical mechanism of the nervous system can improve the motor ability of robots.

VI. CONCLUSION

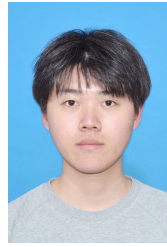
Pre-training reinforcement learning has shown excellent performance in robot motor control. This article presents a novel CMSRL algorithm based on the structure of the CMS. Our learning framework can enable robots to exhibit motor learning abilities similar to those of animals. Through pre-training, the low-level policy can enable different types of robots to acquire basic motor regulation abilities. Through task-training,

robots can quickly adapt to various downstream tasks. In addition, we propose a skill activity calculation function based on the mechanism of the basal ganglia, which can enable robots to autonomously generate motor willingness. And a skill encoding method with skill diverse objective is proposed to improve the independence between skills. We demonstrate the rationality of the algorithm components through theoretical analysis and experiments. Furthermore, compared to baselines, our algorithm demonstrate excellent performance in various robot and task environments. As for future works, combining CMSRL with CPG control methods [43] [44] based on spinal reflex mode is an interesting direction.

REFERENCES

- [1] R. S. Sutton and A. G. Barto, *Reinforcement learning: An introduction*. MIT press, 2018.
- [2] W. Zhu, X. Guo, D. Owaki *et al.*, “A survey of sim-to-real transfer techniques applied to reinforcement learning for bioinspired robots,” *IEEE Transactions on Neural Networks and Learning Systems*, vol. 34, no. 7, pp. 3444–3459, 2023.
- [3] Y. Wang, C. Tang, S. Wang *et al.*, “Target tracking control of a biomimetic underwater vehicle through deep reinforcement learning,” *IEEE Transactions on Neural Networks and Learning Systems*, vol. 33, no. 8, pp. 3741–3752, 2022.
- [4] C. Xiao, P. Lu, and Q. He, “Flying through a narrow gap using end-to-end deep reinforcement learning augmented with curriculum learning and sim2real,” *IEEE Transactions on Neural Networks and Learning Systems*, vol. 34, no. 5, pp. 2701–2708, 2023.
- [5] Y. Li, T. Qi, Z. Ma *et al.*, “Seeking a hierarchical prototype for multimodal gesture recognition,” *IEEE Transactions on Neural Networks and Learning Systems*, pp. 1–12, 2023.
- [6] S. Pateria, B. Subagdja, A.-h. Tan *et al.*, “Hierarchical reinforcement learning: A comprehensive survey,” *ACM Computing Surveys (CSUR)*, vol. 54, no. 5, pp. 1–35, 2021.
- [7] Z. Bing, L. Knak, L. Cheng *et al.*, “Meta-reinforcement learning in nonstationary and nonparametric environments,” *IEEE Transactions on Neural Networks and Learning Systems*, pp. 1–15, 2023.
- [8] J. Gehring, G. Synnaeve, A. Krause *et al.*, “Hierarchical skills for efficient exploration,” *Advances in Neural Information Processing Systems*, vol. 34, pp. 11 553–11 564, 2021.
- [9] X. B. Peng, Y. Guo, L. Halper *et al.*, “Ase: Large-scale reusable adversarial skill embeddings for physically simulated characters,” *ACM Transactions On Graphics (TOG)*, vol. 41, no. 4, pp. 1–17, 2022.
- [10] M. Bear, B. Connors, and M. A. Paradiso, *Neuroscience: exploring the brain, enhanced edition: exploring the brain*. Jones & Bartlett Learning, 2020.
- [11] E. V. Evars, “Brain mechanisms in movement,” *Scientific American*, vol. 229, no. 1, pp. 96–103, 1973.
- [12] P. J. Whelan, “Control of locomotion in the decerebrate cat,” *Progress in neurobiology*, vol. 49, no. 5, pp. 481–515, 1996.
- [13] R. David McK, “Certain aspects of the behavior of decorticate cats,” *Psychiatry*, vol. 1, no. 3, pp. 339–345, 1938.
- [14] I. Bar-Gad, G. Morris, and H. Bergman, “Information processing, dimensionality reduction and reinforcement learning in the basal ganglia,” *Progress in neurobiology*, vol. 71, no. 6, pp. 439–473, 2003.
- [15] A. M. Graybiel, “The basal ganglia,” *Current biology*, vol. 10, no. 14, pp. R509–R511, 2000.
- [16] H. Liu and P. Abbeel, “Behavior from the void: Unsupervised active pre-training,” *Advances in Neural Information Processing Systems*, vol. 34, pp. 18 459–18 473, 2021.
- [17] X. Qu, A. Gupta, Y.-S. Ong *et al.*, “Adversary agnostic robust deep reinforcement learning,” *IEEE Transactions on Neural Networks and Learning Systems*, vol. 34, no. 9, pp. 6146–6157, 2023.
- [18] R. Pina, V. D. Silva, J. Hook *et al.*, “Residual q-networks for value function factorizing in multiagent reinforcement learning,” *IEEE Transactions on Neural Networks and Learning Systems*, pp. 1–11, 2022.
- [19] S. Park, J. Choi, J. Kim *et al.*, “Lipschitz-constrained unsupervised skill discovery,” in *International Conference on Learning Representations*, 2021.
- [20] B. Eysenbach, J. Ibarz, A. Gupta *et al.*, “Diversity is all you need: Learning skills without a reward function,” in *International Conference on Learning Representations*, 2019.

- [21] H. Liu and P. Abbeel, "Aps: Active pretraining with successor features," in *International Conference on Machine Learning*, 2021, pp. 6736–6747.
- [22] S. Hansen, W. Dabney, A. Barreto *et al.*, "Fast task inference with variational intrinsic successor features," in *International Conference on Learning Representations*, 2019.
- [23] D. Pathak, P. Agrawal, A. A. Efros *et al.*, "Curiosity-driven exploration by self-supervised prediction," in *International conference on machine learning*, 2017, pp. 2778–2787.
- [24] R. Sekar, O. Rybkin, K. Daniilidis *et al.*, "Planning to explore via self-supervised world models," in *Proceedings of the 37th International Conference on Machine Learning*, 2020, pp. 8583–8592.
- [25] H. Shi, B. Zhou, H. Zeng *et al.*, "Reinforcement learning with evolutionary trajectory generator: A general approach for quadrupedal locomotion," *IEEE Robotics and Automation Letters*, vol. 7, no. 2, pp. 3085–3092, 2022.
- [26] Z. Bing, E. Álvarez, L. Cheng *et al.*, "Robotic manipulation in dynamic scenarios via bounding-box-based hindsight goal generation," *IEEE Transactions on Neural Networks and Learning Systems*, vol. 34, no. 8, pp. 5037–5050, 2023.
- [27] A. Modares, N. Sadati, B. Esmaceli *et al.*, "Safe reinforcement learning via a model-free safety certifier," *IEEE Transactions on Neural Networks and Learning Systems*, pp. 1–10, 2023.
- [28] S. Park, H. Ryu, S. Lee *et al.*, "Learning predict-and-simulate policies from unorganized human motion data," *ACM Transactions on Graphics (TOG)*, vol. 38, no. 6, pp. 1–11, 2019.
- [29] X. B. Peng, G. Berseth, K. Yin *et al.*, "Deeploco: Dynamic locomotion skills using hierarchical deep reinforcement learning," *ACM Transactions on Graphics (TOG)*, vol. 36, no. 4, pp. 1–13, 2017.
- [30] D. Barber and F. Agakov, "The im algorithm: a variational approach to information maximization," *Advances in neural information processing systems*, vol. 16, no. 320, p. 201, 2004.
- [31] K. Amunts, "Brodmann areas," *Encyclopedia of Evolutionary Psychological Science*, pp. 821–824, 2021.
- [32] M. Weinrich and S. P. Wise, "The premotor cortex of the monkey," *Journal of Neuroscience*, vol. 2, no. 9, pp. 1329–1345, 1982.
- [33] A. V. Kravitz, B. S. Freeze, P. R. Parker *et al.*, "Regulation of parkinsonian motor behaviours by optogenetic control of basal ganglia circuitry," *Nature*, vol. 466, no. 7306, pp. 622–626, 2010.
- [34] J. Phillips, J. Bradshaw, R. Iansel *et al.*, "Motor functions of the basal ganglia," *Psychological research*, vol. 55, pp. 175–181, 1993.
- [35] J. E. Visser and B. R. Bloem, "Role of the basal ganglia in balance control," *Neural plasticity*, vol. 12, no. 2-3, pp. 161–174, 2005.
- [36] A. Klaus, J. Alves da Silva, and R. M. Costa, "What, if, and when to move: basal ganglia circuits and self-paced action initiation," *Annual review of neuroscience*, vol. 42, pp. 459–483, 2019.
- [37] E. Todorov, T. Erez, and Y. Tassa, "Mujoco: A physics engine for model-based control," in *2012 IEEE/RSJ international conference on intelligent robots and systems*. IEEE, 2012, pp. 5026–5033.
- [38] J. P. G. Vonsattel and M. DiFiglia, "Huntington disease," *Journal of neuropathology and experimental neurology*, vol. 57, no. 5, p. 369, 1998.
- [39] W. Poewe and others, "Parkinson disease," *Nature reviews Disease primers*, vol. 3, no. 1, pp. 1–21, 2017.
- [40] T. Haarnoja, A. Zhou, P. Abbeel *et al.*, "Soft actor-critic: Off-policy maximum entropy deep reinforcement learning with a stochastic actor," in *Proceedings of the 35th International Conference on Machine Learning*, 2018, pp. 1861–1870.
- [41] W. Whitney, R. Agarwal, K. Cho *et al.*, "Dynamics-aware embeddings," in *International Conference on Learning Representations*, 2019.
- [42] L. van der Maaten and G. Hinton, "Visualizing data using t-sne," *Journal of Machine Learning Research*, vol. 9, no. 86, pp. 2579–2605, 2008.
- [43] A. Bonagiri, D. Biswas, and S. Chakravarthy, "Coupled memristor oscillators for neuromorphic locomotion control: Modeling and analysis," *IEEE Transactions on Neural Networks and Learning Systems*, pp. 1–15, 2023.
- [44] J. Homchanthanakul and P. Manoonpong, "Continuous online adaptation of bioinspired adaptive neuroendocrine control for autonomous walking robots," *IEEE Transactions on Neural Networks and Learning Systems*, vol. 33, no. 5, pp. 1833–1845, 2022.



Pei Zhang received the B.Eng. degree from Northeastern University, Shenyang, Liaoning, China, in 2021. He is currently working toward the Ph.D. degree at the State Key Laboratory of Synthetical Automation for Process Industries, Northeastern University, Shenyang, Liaoning, China. His research interests include reinforcement learning, machine learning, and robotics.



Zhaobo Hua received the B.Eng. degree from Northeastern University, Shenyang, Liaoning, China, in 2023. He is currently working toward the Ph.D. degree at the State Key Laboratory of Synthetical Automation for Process Industries, Northeastern University, Shenyang, Liaoning, China. His research interests include reinforcement learning, machine learning, and robotics.



Jinliang Ding (Senior Member, IEEE) received the bachelor's, master's, and Ph.D. degrees in control theory and control engineering from Northeastern University, Shenyang, China, in 2001, 2004, and 2012, respectively.

He is currently a Professor with the State Key Laboratory of Synthetical Automation for Process Industry, Northeastern University. He has authored or coauthored over 100 refereed journal articles and refereed papers at international conferences. He has also invented or co-invented 20 patents. His current research interests include modeling, plant-wide control, optimization for complex industrial systems, stochastic distribution control, and multiobjective evolutionary algorithms and their applications.

Dr. Ding was a recipient of the three First-Prize of Science and Technology Awards of the Ministry of Education in 2006, 2012, and 2018, the International Federation of Automatic Control (IFAC) Control Engineering Practice for 2011–2013 Paper Prize, the National Technological Invention Award in 2013, the National Science Fund for Distinguished Young Scholars in 2015, and the Young Scholars Science and Technology Award of China in 2016. One of his articles published on control engineering practice was selected for the Best Paper Award from 2011 to 2013.